ADVANCED ENERGY MATERIALS
www.advenergymat.de



# A Stretchable Polymer–Carbon Nanotube Composite Electrode for Flexible Lithium-Ion Batteries: Porosity Engineering by Controlled Phase Separation

*Hojun Lee, Jung-Keun Yoo, Jong-Hyun Park, Jin Ho Kim, Kisuk Kang,* and Yeon Sik Jung**

**Flexible energy-storage devices have attracted growing attention with the fast development of bendable electronic systems. However, it still remains a challenge to find reliable electrode materials with both high mechanical flexibility/toughness and excellent electron and lithium-ion conductivity. This paper reports the fabrication and characterization of highly porous, stretchable, and conductive polymer nanocomposites embedded with carbon nanotubes (CNTs) for application in flexible lithium-ion batteries. The systematic optimization of the porous morphology is performed by controllably inducing the phase separation of polymethylmethacrylate (PMMA) in polydimethylsiloxane (PDMS) and removing PMMA, in order to generate well-controlled pore networks. It is demonstrated that the porous CNT-embedded PDMS nanocomposites are capable of good electrochemical performance with mechanical flexibility, suggesting these nanocomposites could be outstanding anode candidates for use in flexible lithium-ion batteries. The optimization of the pore size and the volume fraction provides higher capacity by nearly sevenfold compared to a nonporous nanocomposite.**

## 1. Introduction

Flexible energy-storage devices have received increasing amounts of attention along with the rapid development of portable and bendable electronic systems. Of particular interest are flexible lithium-ion batteries (FLIBs) and supercapacitors due to their broad range of potential application and high energy storage density.[1–9] Recently, several groups have demonstrated promising results in the area of FLIBs using various types of materials.[2–7] For example, the paper–CNT nanocomposites reported by Hu et al. and Pushparaj et al. presented good electrochemical performance levels as well as flexibility.[5–7] More recently, Gwon et al. reported that graphene nanosheets can function excellently as flexible anodes as well as current collectors.[3] However, for the realization of more practical and cost-effective FLIBs, it remains a challenge to find reliable electrode materials with good scalability, high mechanical flexibility/toughness, and excellent electron and lithium-ion conductivity.

Polydimethylsiloxane (PDMS) is the most widely used elastomeric polymer owing to its many advantages, such as extraordinary mechanical flexibility and chemical and thermal stability. Due to these advantages, it has been frequently utilized as substrates, scaffolds, or transfer media for flexible and stretchable devices.[2,9,15] To add electrical conductivity to highly flexible PDMS, there have been attempts to attach CNTs directly onto the surface of PDMS using chemical vapor deposition (CVD).[9] However, due to the extremely low surface energy of PDMS, the adhesion of materials including CNTs, in general, requires rather complex procedures such as a surface modification using UV or plasma beforehand.[10,11] In addition, noncrosslinked PDMS chains can gradually deteriorate the adhesion of any attached materials, resulting in poor long-term reliability.[12–14] On the other hand, it was recently demonstrated that the electrical conductivity of elastomers can be enhanced significantly by simply mixing with highly conductive CNTs instead of attaching conductive materials.[15–18] Very stable electrical conductivity under repetitive stretching was reported by Zhang et al.,[15] opening up the possibility of cost-effective, flexible, and electronically conductive materials.

It is important to note that CNTs can efficiently store lithium ions as an electrode for lithium rechargeable batteries. Extensive research has demonstrated the promising electrochemical properties of CNT electrode, which stem from their excellent lithium-ion storage capacity, light weight, and good electronic conductivity.[19–21] Despite these promising aspects, a simple mixture of

H. Lee, J.-K. Yoo, Prof. Y. S. Jung
Department of Materials Science and Engineering
Korea Advanced Institute of Science and Technology (KAIST)
Daejeon, 305-701, Republic of Korea
E-mail: ysjung@kaist.ac.kr
Dr. J.-H. Park
Material R&D Department
LG Display Co., Ltd.
1007, Paju-si, Gyeonggi-do, 413-811, Republic of Korea
Dr. J. H. Kim
Icheon Branch, Korea Institute of Ceramic Engineering and Technology
Icheon-si, Gyeonggi-do, 467-843, Republic of Korea
Prof. K. Kang
Department of Materials Science and Engineering
Seoul National University
Seoul, 151-742, Republic of Korea
E-mail: matlgen1@snu.ac.kr

DOI: 10.1002/aenm.201100725

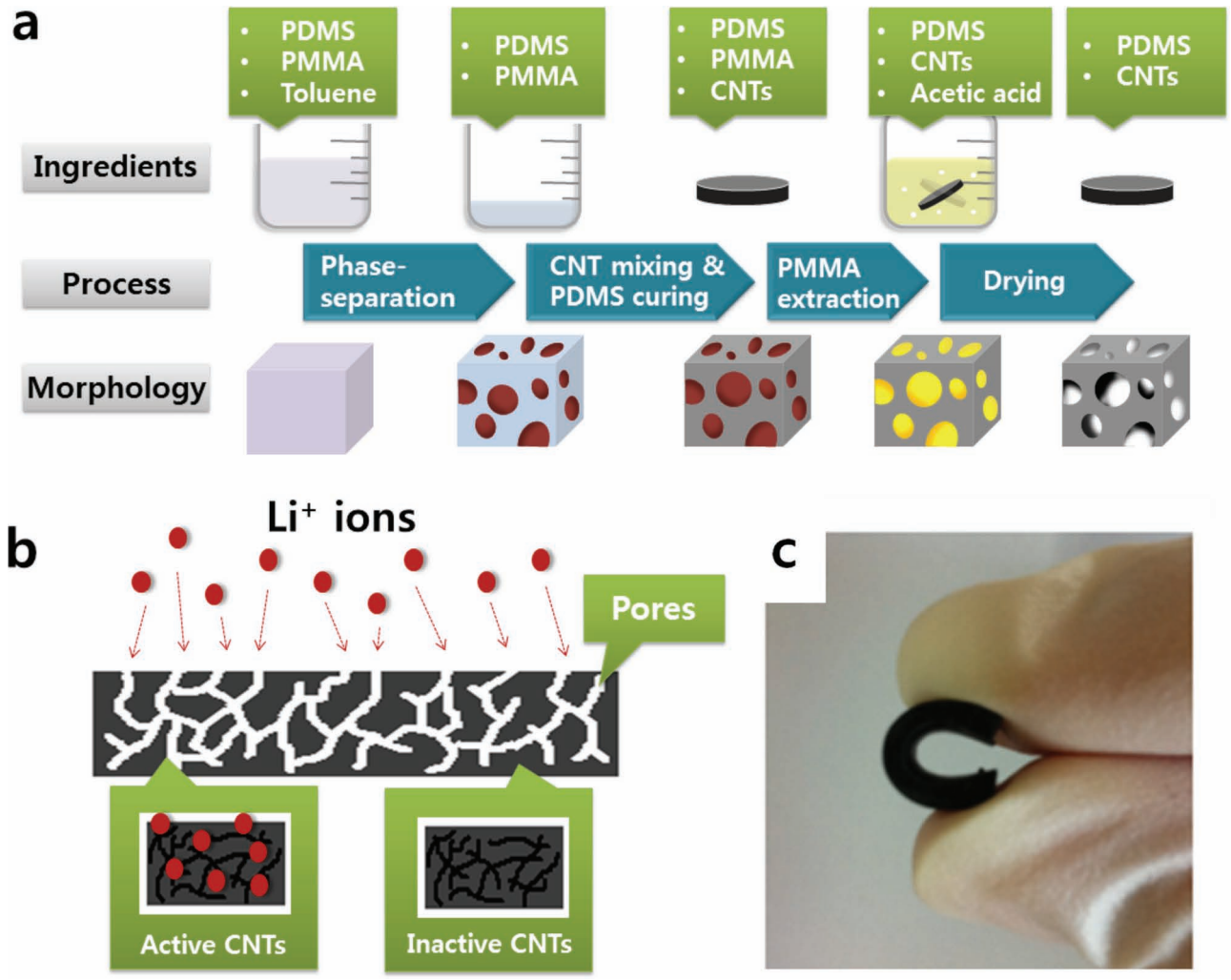


**Figure 1.** a) The procedure to fabricate the porous PDMS–CNT nanocomposites. b) Schematic representation of the PDMS–CNT nanocomposites with porous channels for the effective penetration of electrolytes and lithium ions. c) An example of porous PDMS–CNT nanocomposites demonstrating high mechanical flexibility.

PDMS and CNTs cannot be used as a FLIB electrode, as lithium ions cannot diffuse through the PDMS matrix quickly enough to react with electrochemically active CNTs, as will be discussed in detail in the present study. Therefore, it is critical to engineer facile lithium-ion diffusion pathways artificially within the flexible PDMS matrix. As schematically represented in **Figure 1**b, pores in the PDMS–CNT nanocomposite can serve as interconnected channels through which lithium ions and electrolytes can access the CNTs. One key issue pertaining to the porosity engineering of the nanocomposite involves optimizing the length-scale of the pores so as to maximize the storage capacity while maintaining good mechanical properties.

Here, we introduce a new approach based on the morphological optimization of highly porous PDMS–CNT nanocomposites. In the previous studies mentioned above, the pore sizes in porous energy-storage materials were not controlled or optimized for the best performance as energy-storage electrodes. In this study, the systematic optimization of the porous morphology was performed by controllably inducing the phase separation of polymethylmethacrylate (PMMA) in PDMS and then removing PMMA, in order to generate well-controlled pore networks. We demonstrate that the porous CNT-embedded PDMS nanocomposites are capable of good electrochemical performance with mechanical flexibility, suggesting these nanocomposites could be outstanding anode candidates for use in FLIBs. We achieved an approximately 670% higher storage capacity compared to a nonporous sample by optimizing the scale and distribution of the porous morphology. Moreover, the thickness of the porous electrode can be adjusted over a wide range while maintaining flexibility, providing the capability to extend and control the capacity of flexible batteries easily.

## 2. Results and Discussion

### 2.1. Fabrication of the Porous PDMS/CNT Nanocomposites

Figure 1a schematically illustrates the overall procedure used to fabricate the porous PDMS–CNT nanocomposite. First, PDMS (Sylgard 184, Dow Corning Inc.), PMMA (molecular weight

($M_w$) = 100 kg mol$^{-1}$, Polysciences, Inc.), and PDMS–*b*–PMMA ($M_w$ = 8k–*b*–6k kg mol$^{-1}$, Polymer Source, Inc.) with different mixing ratios were dissolved in toluene at 75 °C. The attainment of good homogeneity in the solution is important, as it can affect the degree of uniformity in the distribution of pores in the nanocomposite after the removal of the PMMA droplets. Toluene was slowly evaporated at 75–105 °C while stirring in order to induce phase separation between PDMS and PMMA. The pore dimension significantly changed depending on the drying temperature and the mixture ratio of the three polymer components. Then, CNTs (diameter = 15 nm) and a curing agent were mixed with the phase-separated PDMS/PMMA blend and annealed at 140 °C for 12 h to crosslink the PDMS and fix the phase-separated morphology. The maximum amount of CNT loading was determined by the solubility limit of the CNTs in the polymer blend. Pristine CNTs can be mixed well with PDMS, but they are repelled by PMMA. Thus, all of the CNTs were preferentially dissolved only in PDMS, and thus the amount of CNTs in the polymer blend decreased with the increasing fraction of PMMA in the mixture. The samples were fully immersed in acetic acid in order to remove PMMA selectively and generate pores, which was followed by washing with deionized water, blowing with nitrogen gas, and drying at an elevated temperature. The porous nanocomposites showed good mechanical flexibility, as shown in Figure 1c.

### 2.2. Key Processing Parameters for Controlling Pore Size and Distribution

Scanning electron microscopy (SEM) images of the porous PDMS–CNT composites are shown in **Figure 2**. The pore diameters significantly varied depending on their preparation conditions. In the initial mixtures of the polymers, the weight mixing ratios of PDMS:PMMA were 80:20 (Figure 2a–d) and 70:30 (Figure 2e–h) and the weight fractions of the block copolymers (PDMS–*b*–PMMA) were 0.02% (Figure 2a,e), 0.1% (Figure 2b,f), 0.2% (Figure 2c,g), and 1% (Figure 2d,h). The CNTs mixed in the porous nanocomposite are shown in the inset of Figure 2a with a higher magnification. All the samples presented in Figure 2 were dried at 75 °C. The SEM images of the nanocomposites prepared with other conditions are shown in Supporting Information (SI), Figure S1,S2.

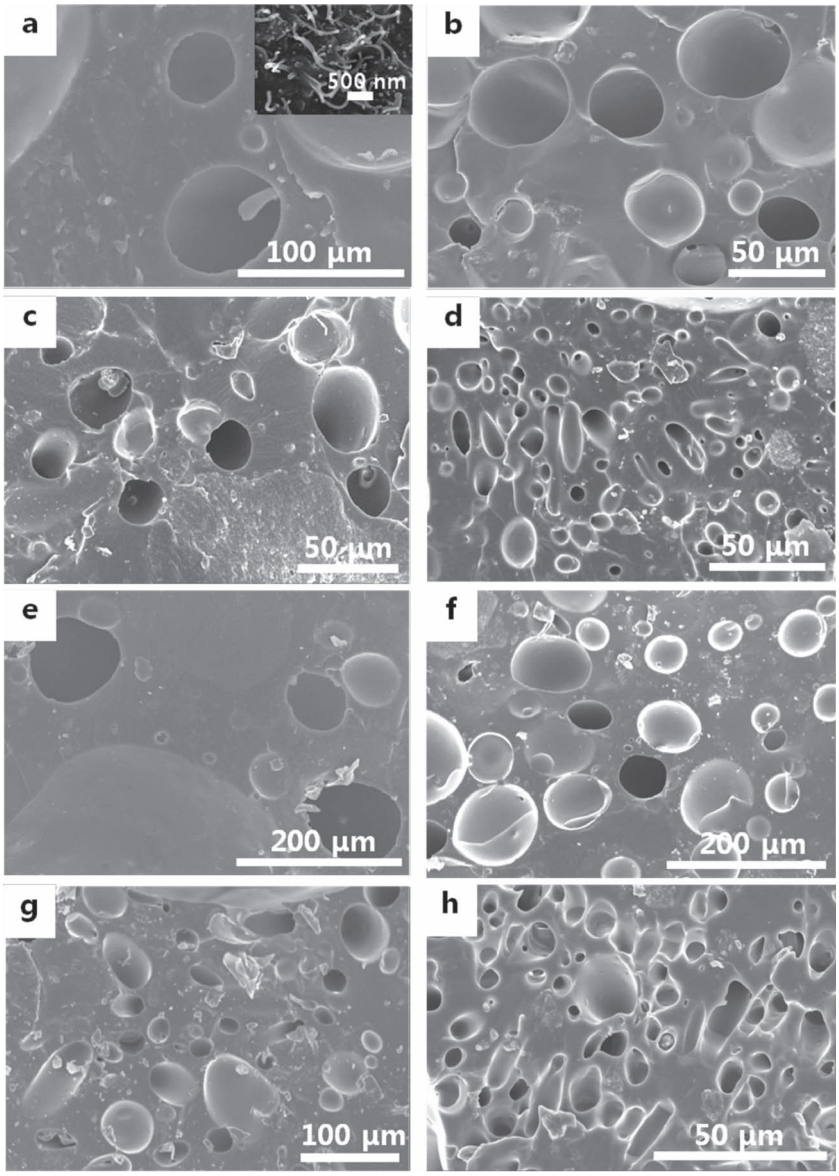


**Figure 2.** SEM images of the porous morphologies of the samples prepared with different fractions of PMMA and the block copolymer in the initial mixture. The weight fraction of the embedded CNTs and the solvent drying temperature were fixed at 5% and 75 °C, respectively. The weight fractions of the PMMA were a–d) 20% and e–h) 30%. The fractions of the PDMS–*b*–PMMA block copolymers were a,e) 0.02, b,f) 0.1, c,g) 0.2%, and d,h) 1%. The inset in (a) shows CNTs loaded in the nanocomposite.

The statistical measurement data for all of the samples are shown in **Figure 3** and **Figure 4**. Figure 3a shows the mass change caused by acetic acid treatments done to remove the PMMA from the polymer blend. It should be noted that the amount of mass reduction is smaller than the actual fraction (approximately 28.5% for the 70:30 samples and 19% for the 80:20 samples) of the PMMA in the blend. This can be attributed to the presence of isolated PMMA droplets which could not be removed by the acetic acid treatment because only interconnected PMMA droplets could be accessed and dissolved by the acid. The mass reduction was most significantly affected by the fraction of PMMA. When the mixing ratio was 70:30, the mass decreased by 19–23%, whereas it decreased by 4–8% for the 80:20 samples. With a higher fraction of PMMA, the probability of interconnection between PMMA droplets may increase, and accordingly more pores can be generated.

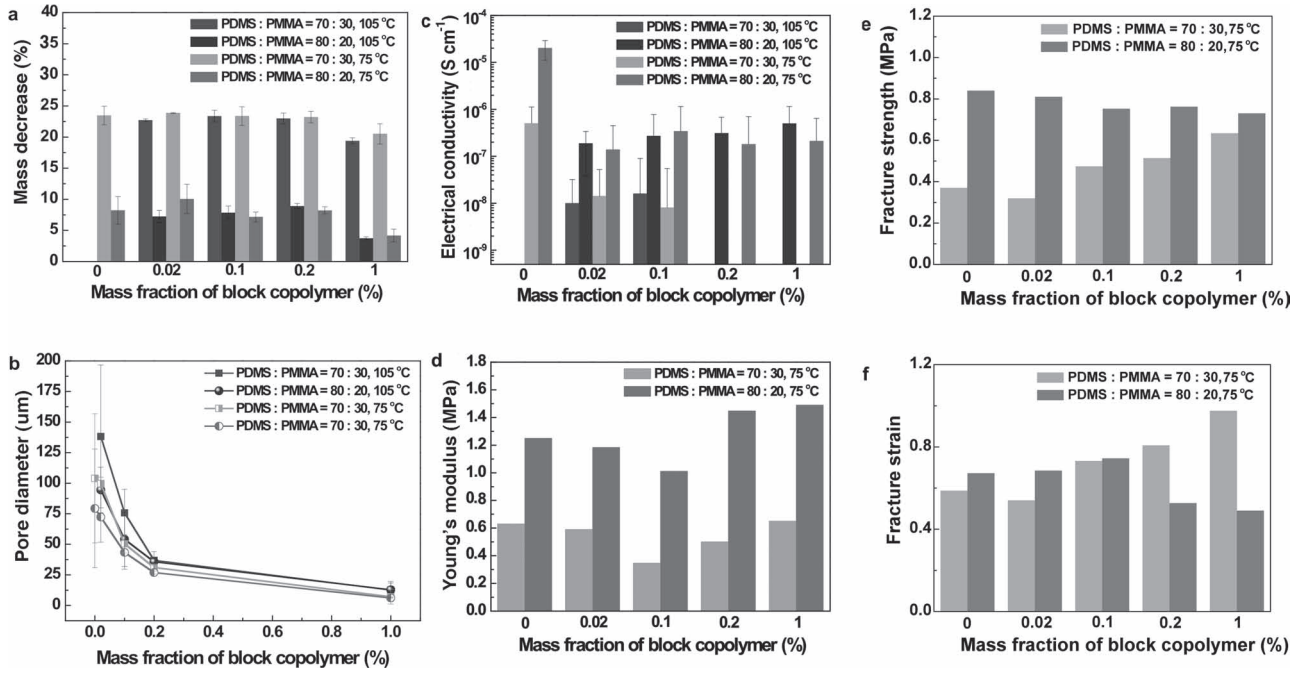


**Figure 3.** Statistical measurement data of a) mass decrease after the removal of the PMMA by an acetic acid treatment, b) diameter of the pores, c) electrical conductivity, d) Young's modulus, e) fracture strength and f) fracture strain depending on the portion of PMMA and PDMS–*b*–PMMA and on the drying temperature. Missing data in (b,c) are due to macroscopic phase separation or because the conductivity was too low.

Phase separation takes place spontaneously during the drying of toluene and the annealing process. The coarsening of PMMA is driven by the reduction of the total interfacial area between the PDMS and the PMMA. As expected, a higher composition of PMMA in the mixture also resulted in larger pores, as shown in the SEM images (Figure 2) and in the graph (Figure 3b). For example, the 70:30 samples without an addition of block copolymers showed approximately 70% larger pore sizes on average compared to the 80:20 samples dried at the same temperature (75 °C). Higher drying temperatures also resulted in considerably larger pores (Figure 3b and SI, Figure S1), which can be understood by the faster growth of the PMMA droplets resulting from the more facile diffusion of the polymer chains. The polymer mixtures without block copolymers were macroscopically separated when they were annealed at 105 °C, and no microscopic pores were observed. However, the addition of the block copolymers (PDMS–*b*–PMMA) was found to decelerate the kinetics of phase separation significantly and reduce the pore size, as shown in Figure 3b, as the block copolymers stabilized the interface between the constituting polymers, resulting in the decreased length scale of the phase-separated morphology.[22–27] This

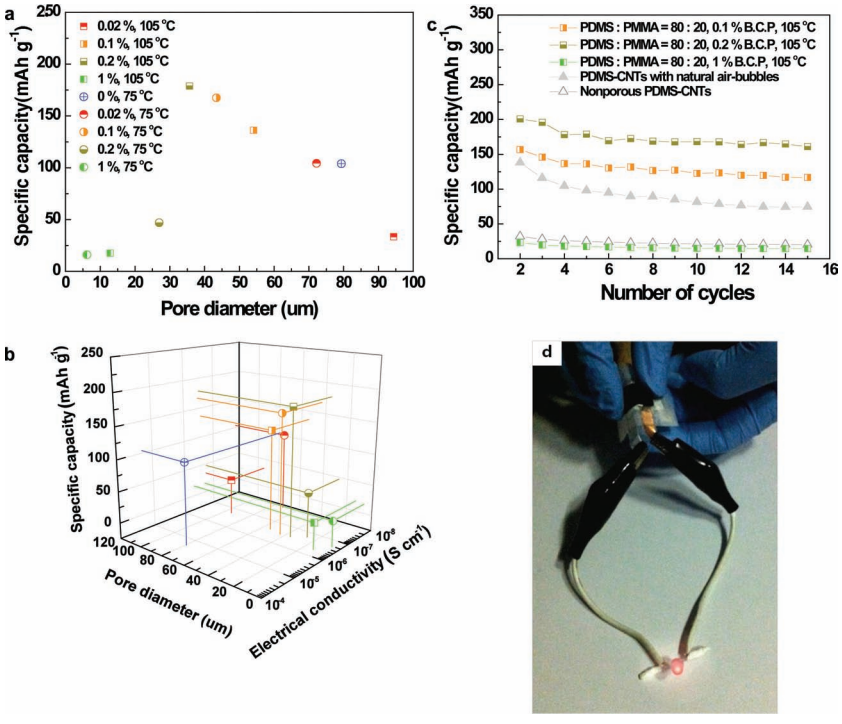


**Figure 4.** a) Capacity per mass of active material of the 80:20 samples depending on the pore size. b) 3D representation of the capacity of the 80:20 samples as a function of pore size and of the electrical conductivity. c) The cycle retention of some 80:20 samples during the first 15 cycles. In (a,b), the values after the fifth cycle are presented. d) A flexible lithium-ion battery full cell fabricated with the porous PDMS–CNT nanocomposites as the anode and $LiCoO_2$ as the cathode.

tendency was consistent at a higher annealing temperature (105 °C). These results suggest that the mixing ratio of PDMS and PMMA, the addition of block copolymers, and the drying temperature are the key parameters controlling the porous morphology of the nanocomposites. With a smaller fraction of PMMA, a higher concentration of the block copolymer, and a lower drying temperature, the pore sizes were observed to be smaller. A wide diameter tuning range between 6–138 μm was achieved by controlling the parameters.

### 2.3. Electrical Conductivity of the Porous Nanocomposites

In addition to the generation of pores for the penetration of lithium ions and electrolytes, assuring high electrical conductivity is important to ensure usability as a practical energy-storage electrode for FLIBs. The electronic percolation of CNTs is known to be responsible for the conductivity of polymer composites embedded with CNTs.[16–18] The concentration and dispersion of CNTs and the fractions and size of pores can collectively affect the degree of percolation and consequently their electrical properties. The measured conductivities of the samples are represented in Figure 3c. All of the samples containing pores showed conductivity lower than $10^{-3}$ S $cm^{-1}$ of the nonporous composite. To begin with, we found that the conductivity of the porous nanocomposites is highly dependent on the fraction of the PMMA in the initial mixture and the scale of pores. As shown in Figure 3c, all of the samples with the mixing ratio of 70:30 showed orders-of-magnitude smaller conductivity compared to the 80:20 samples. With an increase in the fraction of the PMMA, with which CNTs cannot be mixed, the percolation probability of the CNT networks in the porous nanocomposite may decrease. On the other hand, the scale of pores also resulted in a large difference in the conductivity. For the samples with finer pores, as prepared by mixing more block copolymers, the measured conductivities were significantly lower. If the pore sizes are small and the pore volume fractions are high, CNTs cannot maintain their linear shapes because their lengths (~15–20 μm) are larger than the spacing between the pores. For example, the average pore diameter and pore-to-pore spacing for the 1% block copolymer-added 70:30 sample dried at 75 °C were 12.8 μm and 9.5 μm, respectively, which were smaller than the typical lengths of CNTs used in the experiments. Therefore, they should be trapped in local regions owing to blocking caused by the densely distributed PMMA droplets. On the other hand, the formation of larger pores increases the pore-to-pore spacing. As a result, the percolation probability is affected less. The 70:30 samples mixed with 1% block copolymers were almost non-conducting and consequently inappropriate as an electrode for FLIBs. However, other samples showed adequate conductivities, enabling the PDMS–CNT porous nanocomposites to be feasible for use in FLIBs.

### 2.4. Mechanical Properties of the Porous Nanocomposites

Assuring good mechanical properties of porous nanocomposite should also be considered as an important factor. Figure 3d–f present the Young's moduli, fracture strengths, and maximum strains of the PDMS–CNT nanocomposites (drying temperature = 75 °C). Compared to the 70:30 samples, the 80:20 samples showed consistently higher Young's moduli and fracture strengths. In addition to smaller pore volume fractions, the 80:20 samples contained significantly more unremoved PMMA droplets with much higher mechanical stiffness (Young's modulus ~ 1800–3100 MPa) compared to that (1.8 MPa) of PDMS. The relatively high mechanical rigidity of the 80:20 samples can be attributed to the lower pore volume fractions, the smaller pore sizes, and the higher PMMA content. The maximum strain that can be endured by the porous nanocomposites also varied depending on the compositions of the polymers in the initial mixtures. Upon decreasing the size of the pores by increasing the fraction of the block copolymer, the 70:30 samples showed increasing fracture strains as well as fracture strengths, which may be due to the easier initiation of cracks from the larger pores. However, for the 80:20 specimens, the fracture strengths and strains were relatively low for smaller pores, most likely because the finely distributed PMMA droplets in the PDMS matrices make them more brittle. Overall, for the samples with at least moderate charge storage capacities, which will be discussed in detail in the next part, the mechanical toughness was relatively high for the 80:20 samples and relatively small for the samples with larger pores. A few examples of the stress–strain curves of the nanocomposites are shown in SI, Figure S3.

### 2.5. Electrochemical Properties of the Porous Nanocomposites

The electrochemical performances of the porous nanocomposites were evaluated, as shown in Figure 4a–c and in SI, Figure S5a,b. The pore size and distribution as well as the electrical conductivity were found to affect the specific capacity of the samples collectively, as shown in Figure 4b. The specific capacity was calculated by dividing the measured absolute capacity by the mass of the CNTs added to the nanocomposite. As a reference, a sample with no pores was prepared without mixing PMMA, with degassing done in a vacuum for 20 min. Another sample processed without the degassing step had naturally occurring pores with a diameter of hundreds of micrometers, but the number density of the pores was much lower than those of other samples prepared by phase separation. We found that the existence of pores significantly enhanced the specific capacity of the samples. The nonporous sample had a specific capacity of (20 mAh $g^{-1}$), which is much lower than that (75 mAh $g^{-1}$) of the sample with natural pores. This difference can be explained by the hypothesis that lithium ions and electrolytes cannot penetrate deep into a nanocomposite without pores.

Next, we demonstrate how the capacity of the porous nanocomposites can be significantly enhanced or deteriorated depending on the size and distribution of the pores. For the same pore volume fractions, the total pore surface area will be higher with smaller pores, which then results in a higher portion of CNTs coming into direct contact with the electrolyte absorbed by the nanocomposites through the pores. However, the pores also affect the percolation behavior in the CNT network, as confirmed by the dramatic decrease in the electrical conductivity upon a decrease in the size of pores and an increase in the volume fraction of the pores. With the CNT

networks better connected, the fraction of isolated and inactive CNTs will be smaller and thus the specific capacity will be higher. Another governing factor is the effectiveness of electrolyte infiltration through the pore networks. Because the PDMS surface exhibits strong hydrophobicity, it can impede the penetration of the electrolytes (the mixture of ethylene carbonate and dimethyl carbonate), which is much less hydrophobic, through narrow pore channels. These mutually opposing effects propose the existence of an optimum pore size which maximizes the storage capacity.

As shown in Figure 4a,b (80:20 mixtures) and SI, Figure S5a (70:30 mixtures), the samples with moderate pore sizes (diameter ~ 30–60 μm), as prepared by mixing 0.1–0.2% of block copolymers, possessed higher capacities. The occurrence of the maximum capacity with relatively higher pore sizes for the 70:30 samples can be attributed to the larger pore fractions and smaller pore-to-pore distance, which together reduce the degree of percolation in the CNT networks. Thus, these samples require relatively more coarsened structures to obtain both high electronic conductivity and sufficient electrolyte penetration. As was discussed earlier, the samples with moderate pore sizes also presented excellent mechanical stretchability with a fracture strain of larger than 70%. The extremely fine morphology (pore diameter ~ 6–8 μm) resulted in a capacity even smaller than that of the nonporous sample, which can be explained by the extremely poor electrical conductivity and electrolyte permeation. In fact, the weight increase of the nanocomposites caused by the absorption of the electrolytes was higher when the pore size was moderate (pore diameter ~ 30–50 μm) and decreased significantly with larger and smaller pore sizes. The 80:20 nanocomposites showed usually higher capacities in comparison to the 70:30 samples. This may be related to the better electrical percolation in the CNTs due to less hindrance by the pores, which is supported by the higher conductivity shown in Figure 3c. The porosity-optimized nanocomposite showed almost 670% larger capacity compared to the nonporous sample. The highest capacity per weight of active material was 160–190 mAh $g^{-1}$, which is around 64–76% of experimentally measured capacity of typical CNT powders, suggesting that a more finely tuned optimization process may be able to increase the capacity of the porous nanocomposites even further. The maximum specific capacity calculated based on the complete nanocomposite (PDMS + CNT) was estimated to be around 7 mAh $g^{-1}$, which is considerably smaller than those of conventional CNT powders. However, the porous and conductive polymer/CNT nanocomposite does not require additional current collectors made of metals such as Cu; thus, the energy storage density of a full-cell device can be significantly enhanced. The cycle retention characteristics of the 80:20 samples are shown in Figure 4c. Additional cycle retention measurement data for the 70:30 samples and exemplary charge–discharge curves are available in SI, Figure S4,S5. The nanocomposites with the highest capacities showed stable retention characteristics up to more than tens of cycles. The porous nanocomposites can serve as an anode for an FLIB under bending. A red light-emitting diode was successfully operated by a test FLIB (bending radius range of ~4.5 mm) based on the porous PDMS–CNT nanocomposite as shown in Figure 4d.

## 3. Conclusion

Highly porous and flexible PDMS–CNT nanocomposites were successfully fabricated and their porosity was optimized by controlling the degree of phase separation between PDMS and PMMA. We demonstrated that their charge storage capacities can vary significantly depending on the scale and fraction of the pores, which can be controlled by adjusting the key processing parameters such as the polymer mixing ratio of the PDMS, PMMA, and block copolymers and the drying temperature of the mixed solution. With a smaller fraction of PMMA, a higher concentration of block copolymer, and a lower drying temperature, the pore sizes were observed to be smaller. The electrical conductivity dramatically decreased upon increasing the pore volume fraction and decreasing the pore size. Both the electrochemical performance levels as well as the mechanical properties were superior in the nanocomposites with moderate pore sizes, which may provide relatively more favorable conditions for the penetration of electrolytes and the interconnections among CNTs. The porosity-optimized nanocomposite showed 670% higher capacity compared to a nonporous nanocomposite, showing that this example of morphological engineering will be highly useful for realizing more practical flexible energy-storage devices.

## 4. Experimental Section

*Sample Preparation*: PDMS (Sylgard 184), PMMA ($M_W$ = 100 kg $mol^{-1}$), PDMS–*b*–PMMA block copolymer ($M_W$ = 8–*b*–6 kg $mol^{-1}$) and multiwalled carbon nanotubes were purchased from Dow Corning, Polysciences, Inc., Polymer Source, Inc. and Hanwha Nanotech, respectively. The composition ratios of the PDMS/PMMA blends were 70/30 or 80/20 by weight. The weight fraction of the added block copolymers was 0–1%. The polymers were dissolved in toluene (Sigma Aldrich) at 75 °C for 6 h, after which the solvent was slowly evaporated while stirring at 75–105 °C, depending on the samples, in order to induce the phase separation between the PDMS and the PMMA. CNTs and a curing agent were added to the PDMS/PMMA blends and mixed sufficiently after the toluene was fully dried. CNTs should be added after phase separation in order to prevent the partial separation of CNTs from the polymer blends during the drying process. For all of the samples, the weight ratios of the PDMS base/curing agent and PDMS/CNT were 10:1 and 20:1, respectively. The black polymer/CNT mixtures were cured at 140 °C for 12 h. Finally, the composites cut down to pieces of a thickness of 1 mm and were fully immersed in acetic acid (Junsei Chemical Co., Ltd) under sonication for 99 min, which was followed by drying at 120 °C for 2 h. The acetic acid treatment also selectively removed the PMMA block in the block copolymer added in the polymer blend.

*Characterization*: Mass changes were measured by weighing the samples before and after the PMMA extraction step. The porous morphology was characterized using a Hitachi S-4800 FESEM with an acceleration voltage of 10.0 kV. The pore sizes were calculated with image analysis software (Image J). The mechanical properties were characterized using a universal testing machine (INSTRON 5583) with a tension rate of 1 mm $min^{-1}$. The electrochemical characterization processes were performed using two-electrode Swagelok-type cells (3 × 3 × 1 $mm^3$) with lithium metal (Hohsen Corp.) as a counter electrode. The cells were also used for the measurement of electrical conductivity using a digital multimeter. The electrolyte employed was 1 M of $LiPF_6$ in a 1:1 mixture of ethylene carbonate and dimethyl carbonate (Techno Semichem Co., Ltd.). A porous membrane (Celgard 2400) was used as a separator. The cells were assembled in an Ar-filled glove box. The discharge and charge measurements were carried out at 18.615 mA $g^{-1}$

within a voltage window of 0.01–3.0 V on a battery test system (Won-A Tech).

## Supporting Information

Supporting Information is available from the Wiley Online Library or from the author.

## Acknowledgements

This work was financially supported from the National Research Foundation of Korea (NRF) grant funded by the Korea government (MEST) (No. 2011-0026121, No.2011-0007183, and 2011K000691) and from Green Smart Card Platform Technologies Based on 3D Printed Electronic Devices Project (B551179-09-07) of MKE (Ministry of Knowledge Economy) and ISTK (Korea Research Council for Industrial Science and Technology).

Received: November 29, 2011
Revised: December 22, 2011
Published online: April 2, 2012

[1] J. M. Tarascon, M. Armand, *Nature* **2001**, *414*, 359.
[2] Y. Yang, S. Jeong, L. B. Hu, H. Wu, S. W. Lee, Y. Cui, *Proc. Natl. Acad. Sci. USA* **2011**, *108*, 13013.
[3] H. Gwon, H. S. Kim, K. U. Lee, D. H. Seo, Y. C. Park, Y. S. Lee, B. T. Ahn, K. Kang, *Energy Environ. Sci.* **2011**, *4*, 1277.
[4] A. Goyal, A. L. M. Reddy, P. M. Ajayan, *Small* **2011**, *7*, 1709.
[5] L. B. Hu, H. Wu, F. La Mantia, Y. A. Yang, Y. Cui, *ACS Nano* **2010**, *4*, 5843.
[6] L. B. Hu, J. W. Choi, Y. Yang, S. Jeong, F. La Mantia, L. F. Cui, Y. Cui, *Proc. Natl. Acad. Sci. USA* **2009**, *106*, 21490.
[7] V. L. Pushparaj, M. M. Shaijumon, A. Kumar, S. Murugesan, L. Ci, R. Vajtai, R. J. Linhardt, O. Nalamasu, P. M. Ajayan, *Proc. Natl. Acad. Sci. USA* **2007**, *104*, 13574.
[8] Z. Weng, Y. Su, D. W. Wang, F. Li, J. H. Du, H. M. Cheng, *Adv. Energy Mater.* **2011**, *1*, 917.
[9] C. J. Yu, C. Masarapu, J. P. Rong, B. Q. Wei, H. Q. Jiang, *Adv. Mater.* **2009**, *21*, 4793.
[10] J. A. Vickers, M. M. Caulum, C. S. Henry, *Analyt. Chem.* **2006**, *78*, 7446.
[11] J. Kim, M. K. Chaudhury, M. J. Owen, T. Orbeck, *J. Colloid Interface Sci.* **2001**, *244*, 200.
[12] J. Kim, M. K. Chaudhury, M. J. Owen, *J. Colloid Interface Sci.* **2000**, *226*, 231.
[13] D. C. Duffy, J. C. McDonald, O. J. A. Schueller, G. M. Whitesides, *Analyti. Chem.* **1998**, *70*, 4974.
[14] J. L. Fritz, M. J. Owen, *J. Adhesion* **1995**, *54*, 33.
[15] Y. Y. Zhang, C. J. Sheehan, J. Y. Zhai, G. F. Zou, H. M. Luo, J. Xiong, Y. T. Zhu, Q. X. Jia, *Adv. Mater.* **2010**, *22*, 3027.
[16] T. P. Chua, M. Mariatti, A. Azizan, A. A. Rashid, *Compos. Sci. Technol.* **2010**, *70*, 671.
[17] Y. Mamunya, A. Boudenne, N. Lebovka, L. Ibos, Y. Candau, M. Lisunova, *Compos. Sci. Technol.* **2008**, *68*, 1981.
[18] A. Allaoui, S. Bai, H. M. Cheng, J. B. Bai, *Compos. Sci. Technol.* **2002**, *62*, 1993.
[19] S. W. Kim, D. H. Seo, H. Gwon, J. Kim, K. Kang, *Adv. Mater.* **2010**, *22*, 5260.
[20] S. W. Kim, J. Ryu, C. B. Park, K. Kang, *Chem. Commun.* **2010**, *46*, 7409.
[21] R. S. Morris, B. G. Dixon, T. Gennett, R. Raffaelle, M. J. Heben, *J. Power Sources* **2004**, *138*, 277.
[22] J. A. Galloway, H. K. Jeon, J. R. Bell, C. W. Macosko, *Polymer* **2005**, *46*, 183.
[23] C. Harrats, T. Omonov, G. Groeninckx, P. Moldenaers, *Polymer* **2004**, *45*, 8115.
[24] C. Harrats, R. Fayt, R. Jerome, S. Blacher, *J. Polym. Sci. Pol. Phys.* **2003**, *41*, 202.
[25] S. Lyu, T. D. Jones, F. S. Bates, C. W. Macosko, *Macromolecules* **2002**, *35*, 7845.
[26] H. Retsos, I. Margiolaki, A. Messaritaki, S. H. Anastasiadis, *Macromolecules* **2001**, *34*, 5295.
[27] C. Verdier, H. T. M. Vinagre, M. Piau, D. D. Joseph, *Polymer* **2000**, *41*, 6683.